Advanced Laboratory Course

– A245: Optical Frequency doubling –

Supervisor
Till Ockenfels

Summer Term 2017

Abstract

The aim of this experiment is to understand the properties of second harmonic waves as an effect in non-linear optics. Therefore it is crucial to understand the dependence of it to various parameters, which will be tested during the experiment. Also the frequency relation of the second harmonic to its fundamental wave has to be investigated.
For this purpose a potassium niobate crystal ($KNbO_3$) is irradiated with a high-power diode laser at 987 nm to observe the frequency doubling. The dependence of the second harmonic generation on various parameters is investigated. Two different methods to determine the frequency relation of the two waves are applied.

Contents

1 Theory

In this section the most important theoretical concepts of this experiment will be presented. Further details to this can be found in the standard literature.

1.1 Diode laser

A diode laser consists of a *pn*-junction that is pumped with a voltage, such that electron-hole-pairs will recombine and emit a photon of a fixed energy. This energy is exactly given by the band gap of the material. After this junction a resonator is built up to achieve stimulated emission in the material such that the output has the property that all photons share the same phase, or in lay man's terms that the output radiation can be classified as laser light.

1.2 Generation of higher harmonics

Before the invention of the laser and thus of light sources with arbitrarily high intensities one could only observe linear effects when irradiating material, e.g. diffraction described by Snellius' law. The classification of such processes as *linear* emerges from the fact that they can mathematically be described by a linear dependence of the polarization vector $\mathbf{P}$ on the electric field $\mathbf{E}$. Here the light stimulates small oscillations of the electrons in the material, such that they see only the harmonic potential of one nucleus, however with rising beam intensity the oscillations also increase. In this case the description with a purely harmonic potential breaks down since the influence of surrounding nuclei can no longer be omitted. Thus the potential gets anharmonic and the relation of the polarization and the electric field is not linear any more, but can be expressed using an expansion in the field:

$$\mathbf{P} = \epsilon_0 \sum_n \chi^{(n)} \prod_j^n \mathbf{E_j} = \epsilon_0 \left(\chi^{(1)}\mathbf{E} + \chi^{(2)}\mathbf{E_1}\mathbf{E_2} + \mathcal{O}(\mathbf{E^3}) \right) \tag{1}$$

Here $\chi^{(1)}$ is the well-known susceptibility from linear optics. One can generalize this to higher order processes by choosing $\chi^{(n)}$ to be a rank-$(n+1)$-tensor. Assuming the incoming electric field is a plane wave with $\mathbf{E} = E_0 \sin(\omega t)$ the second order polarization vector reads:

$$P^{(2)} = \epsilon_0 E_0^2 \chi^{(2)} \sin^2(\omega t) = \Delta P^{(2)} - \Delta P^{(2)} \cos(2\omega t) \tag{2}$$

where $\Delta P^{(2)}$ is just a constant. From this it is obvious that a high intensity beam will lead to two non-linear effects which can be interpreted as a polarization of the material and the generation of light with the doubled frequency. In our case we only couple one fundamental wave into the medium, one could think of coupling different beams to it. This would lead two secondary beams with the difference and sum of the frequencies. From now on the incoming wave will be called the fundamental wave while the generated wave with the doubled frequency will be called second harmonic wave.

The intensity of the second harmonic wave is given by

$$I_{\mathrm{SH}} = \Gamma^2 L^2 I_{\mathrm{FUN}}^2 \operatorname{sinc}^2(\Delta k L) \tag{3}$$

where Γ is a material constant, L the length of the crystal in which the generation takes place and $\Delta k = \frac{2\omega}{\mathrm{c}}(n(2\omega) - n(\omega))$ the phase mismatch [LSP]. This phase mismatch occurs due to the fact that the refractive index is a strictly monotone function of the frequency. Hence it is crucial to perform a so called phase matching to optimize the intensity of the second harmonic. All methods to achieve phase matching that will be introduced in this report exploit the properties of uniaxial crystals or birefringence.

1.3 Birefringence

Birefringence is a property of an uniaxial crystal in contrast to optically isotropic media. Such optically isotropic media have the same refractive index in each direction, hence the refractive index is independent of the direction of the incoming wave. This can be seen in the formalism of Jones matrices as a scaled identity matrix. However uniaxial crystals have two refractive indices, called the ordinary n_{o} and the extraordinary index n_{e}, where only one of the three axes in 3D shows the extraordinary one. This axis will be called the optical axis.

Birefringence can occur as negative ($n_{\mathrm{o}} < n_{\mathrm{e}}$) and positive birefringence ($n_{\mathrm{o}} > n_{\mathrm{e}}$), which will be of interest when discussing phase matching. Another property of the birefringence that will be of interest later is the behaviour of the effective refractive index. So far it was only considered that a beam is exactly parallel to one of the possible axes, but if it passes through the crystal with an angle θ w.r.t. the ordinary axis the effective refractive index can be calculated using the following formula:

$$\frac{1}{n_{\mathrm{e}}^2(\theta)} = \frac{\cos^2\theta}{n_{\mathrm{o}}^2} + \frac{\sin^2\theta}{n_{\mathrm{e}}^2} \tag{4}$$

This is called the refractive index ellipsoid [LSP]. Obviously the effective ordinary index, which is the index of the perpendicular axis, can be obtained by switching the sign of the second term.

1.4 Phase matching

As mentioned before the phase matching of the fundamental wave and the second harmonic is a crucial point in this experiment and optical frequency doubling in general. This can be understood by a gedankenexperiment. Imagine that only two photons of the second harmonic will be generated at two different locations in the crystal. Now it is obvious that the phase of the second harmonic is connected to the phase of the fundamental wave. If now the refractive index is such that the first second harmonic travels a full wavelength while the fundamental wave only travels half its wavelength before emitting the second photon of the harmonic wave, the two photons will interact destructively. This argument also holds for the real waves, hence the second harmonic

can only interfere constructively with itself if the phases of the fundamental and harmonic wave are matched.
There are various methods to achieve phase matching. In the course of this report we will concentrate on three possible methods that exploit the birefringence of an uniaxial crystal.

1.4.1 Type I phase matching

In this type of phase matching the orientation of the crystal is chosen in such a way that the second harmonic travels along the axis with the (extra-)ordinary refractive index in case of (negative) positive birefringence, while the fundamental wave travels along the perpendicular axis. This leads to phase matching since $n_{\mathrm{o}}(2\omega) = n_{\mathrm{e}}(\omega)$ (or vice versa) can be achieved by choosing the material constants accordingly.

1.4.2 Type II phase matching

In contrast to type I phase matching this type of phase matching can be performed without having to precisely tuning the material constants. As mentioned before the effective refractive index of an uniaxial crystal is given by eq. 4, which can be interpreted as an ellipsoid. If we now consider the ellipsoids for both the fundamental and harmonic wave, it is possible for them to intersect. These points refer to exact phase matching and can for example be seen in fig. 1. Thus phase matching can be achieved by fine tuning the angle of the crystal

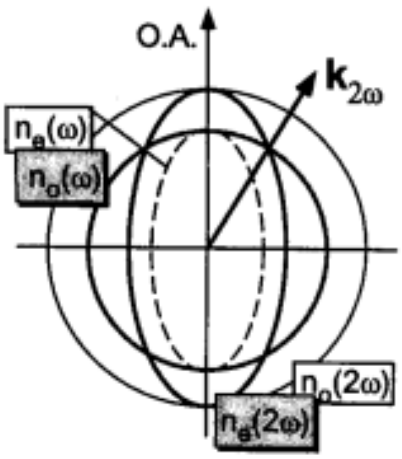

Figure 1: Ellipsoids and intersection points for the fundamental and harmonic beam (taken from [MOLL])

such that one of the possible intersection points is realized. In the case of positive birefringence this can be mathematically formulated as $n_{\mathrm{o}}(2\omega, \theta) = n_{\mathrm{e}}(\omega, \theta)$.

1.4.3 Non-critical phase matching

The formerly discussed ways to achieve phase matching can be classified as critical processes, since they are very sensitive on the angle theta. This makes them harder to achieve than a non-critical way. In this experiment we will

therefore use a non-critical way. To achieve this one starts by applying one of the methods above but not to high precision. The fine tuning is then achieved by adjusting the temperature of the crystal since the refractive indices of most materials also depend on this variable. With this method it is not as difficult to attain phase matching.

1.5 Gaussian beam

A monochromatic beam is called gaussian beam if the distribution of the intensity along any axis perpendicular to its direction can be described using a gaussian distribution. One also speaks of a gaussian profile in this case. Such a beam is characterized by certain variables that can be read off in fig. 2. The

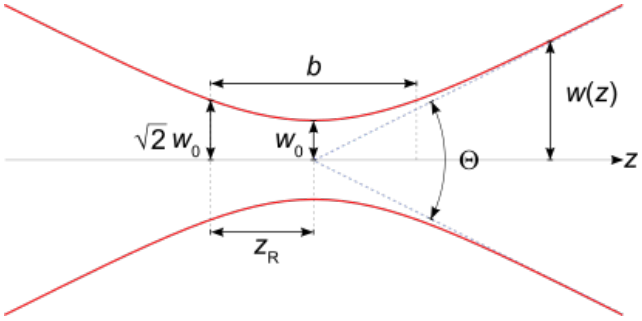

Figure 2: Schematic of the profile of a gaussian beam with highlighted beam variables (taken from [WGB])

parameters that appear here are the beam width in dependence of the travelled distance $w(z)$ and the according minimal beam width w_0, which is also called beam waist. Other parameters that characterize the gaussian beam are the confocal parameter b and the Rayleigh length z_R. As one can see the width of the beam asymptotically approaches a linear function, where one can define the opening angle of this asymptotic behaviour as the beam divergence Θ.
Since the output of most lasers has such a beam profile it is obvious that one can not achieve completely parallel beams over the full crystal length as one can see in fig. 3. There the Rayleigh-length on the right hand side is much smaller than the crystal length, which corresponds to a high intensity in a small region of parallel beams within the crystal. On the left hand side in the same figure

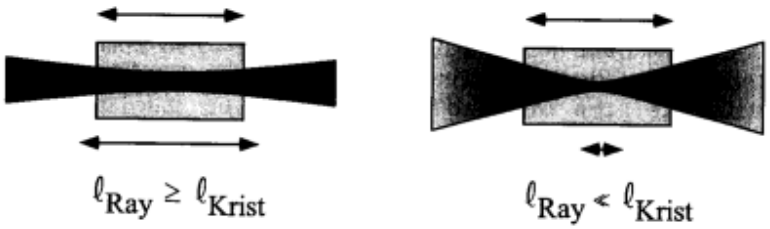

Figure 3: Schematic of the beam within the crystal for different Rayleigh lengths. Due to the poor resolution of the copy the colour coding of the intensity within the crystal can not be seen well. (taken from [MOLL]

one can see the beam profile for a higher Rayleigh length, which corresponds

to nearly parallel beams over the full crystal length with less intensity. It is obvious that here a trade-off between parallel beams and intensity is realized and the issue is to find the optimal region for the second harmonic generation. Optimizing the parameters of SHG w.r.t. to this leads to the so called Boyd-Kleinmann relation. It states that the intensity of the second harmonic can be optimized by choosing the confocal parameter of the fundamental wave such that

$$\frac{L}{b} = 2.84 \tag{5}$$

holds for the used crystal. The derivation of this relation would exceed the scope of this report; it can be found in [MOLL].
In our case[1] the length of the uniaxial crystal is $L = 5\,\mathrm{mm}$ and it has a refractive index $n = (2.2 \pm 0.1)$. We use a lens with focal length $f = 60\,\mathrm{mm}$ and the fundamental wave has a wavelength of $\lambda = 987\,\mathrm{nm}$. With a diameter of the laser before the lens of $d = (3.5 \pm 0.5)\mathrm{mm}$ we get

$$\begin{aligned} w_0 &= \frac{\lambda f}{\pi d/2} \\ &= 10.8\,\mu\mathrm{m} \\ \Delta w_0 &= \frac{2\lambda f \Delta d}{\pi d^2} \\ &= 1.5\,\mu\mathrm{m} \end{aligned}$$

as a minimal beam width and thus the confocal parameter

$$\begin{aligned} b &= \frac{2\pi n w_0^2}{\lambda} \\ &= 1.62\,\mathrm{mm} \\ \Delta b &= \frac{2\pi}{\lambda}\sqrt{\left(\Delta n w_0^2\right)^2 + \left(2 n w_0 \Delta w_0\right)} \\ &= 0.47\,\mathrm{mm}\,. \end{aligned}$$

At last we can check that the Boyd-Kleinman condition in our case

$$\frac{L}{b} = 3.08 \pm 0.89$$

is fulfilled within errors $\Delta\left({}^{L}\!/\!_{b}\right) = {}^{L\Delta b}\!/\!_{b^2}$. The optimal parameters for the fulfilment of the Boyd-Kleinman condition would be:

$$\begin{aligned} b &= \frac{L}{2.84} \\ &= 1.76\,\mathrm{mm} \\ w_0 &= \sqrt{\frac{b\lambda}{2\pi n}} \\ &= 11.2\,\mu\mathrm{m} \\ f &= \frac{\pi d w_0}{2\lambda} \\ &= 62.5\,\mathrm{mm} \end{aligned}$$

[1] Numbers taken from [A245].

1.6 Diffraction Grating

A diffraction grating can be used to measure the wavelength of light, it will later on be used to verify the frequency relation of the fundamental wave and the second harmonic. The cross-section of such a grating can be seen in fig. 4, where also the important angles are defined. This structure of the surface makes the

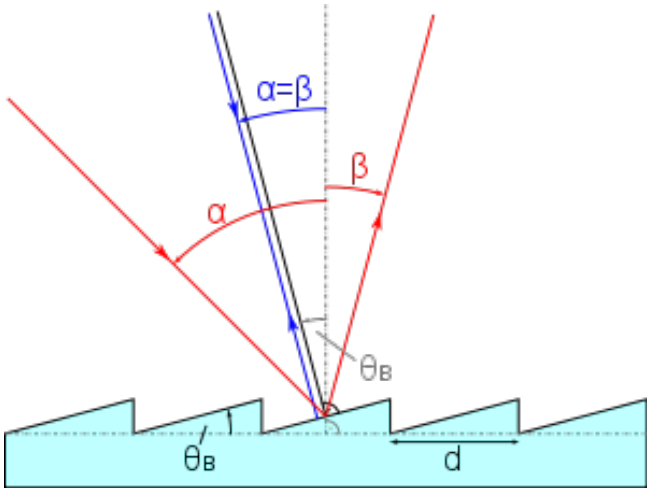

Figure 4: Cross-section of a diffraction grating with important angles and constants (taken from [WikiG])

diffraction of incoming light by the grating dependent on the wavelength, since the outgoing waves will only interfere constructively if the following condition holds:

$$m\lambda = |\sin\alpha - \sin\beta| \cdot d \tag{6}$$

where d is the facet spacing and m the order of the observed maximum. This behaviour should be well known from the double-slit experiment performed by Young. The advantage of a grating compared to a double-slit is the higher resolution that is given by:

$$R = \frac{\lambda}{\Delta\lambda} = m \cdot N \tag{7}$$

where N is the number of illuminated facets on the grating. However it will turn out that this resolution is still to poor to validate the frequency relation of the two beams with satisfactory precision. Hence we will introduce another method in the next section.

1.7 Michelson interferometer

The infamous Michelson interferometer was designed to prove the existence of the aether (see [WAT]) but as we know today was condemned to fail from the very beginning. However it can be used to determine the phase relation of two incoming beams. The schematic of such an interferometer is shown in fig. 5. It is built up using a beam-splitter and two mirrors that are arranged as seen in the figure. Hence an incoming beam will be splitted into two beams that

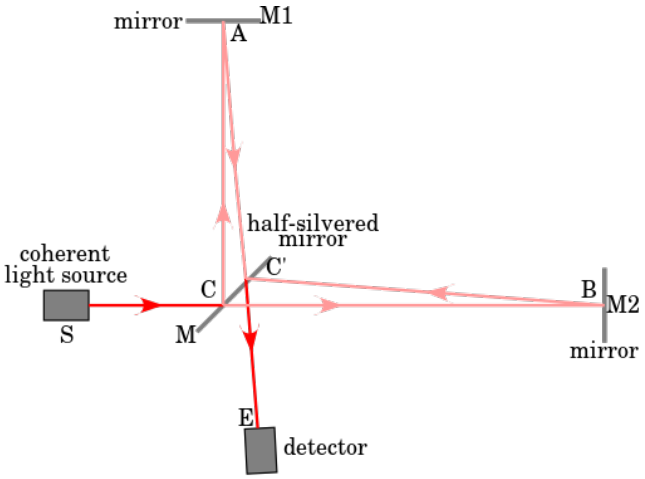

Figure 5: Schematic of a Michelson interferometer (taken from [WiMM])

travel along the perpendicular arms of the interferometer and are reflected on the mirrors respectively. Through the second passing of the beam-splitter they will be brought to interference in the detector. At this point the phase relation of the two beams is only dependent on the length of the arms. Thus by altering the distance of a mirror one can measure the wavelength of the incoming light. It should be mentioned that this requires movements of the mirror in the order of the wavelengths. Obviously we will not be able to perform such movements with a decent precision. In addition we want to measure the wavelength relation of two beams, hence this setup will be extended such that a second beam is brought to interference and measured at a different detector. The signals of those detectors can then be used as x and y-signals for a graph, that will lead to so called Lissajous figures if observed with an oscilloscope. As explained later on this will give a handle on a more precise measurement of the wavelength difference.

1.8 Lissajous figures

Lissajous figures come to existence if one interprets two oscillations as x and y of a graph, which means that the displacements of the two oscillators will be used as coordinates at each time step. If the ratio of the amplitudes of the two oscillations is a rational number the shape that emerges is closed. This can be seen in dependence of the phase shift for the ratio of $1/2$ in fig. 6. Hence

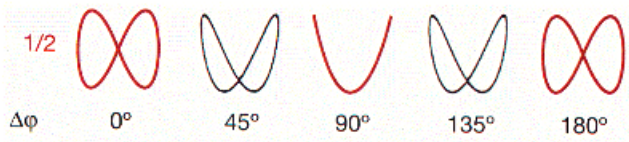

Figure 6: Lissajous figures for different phase shifts with an amplitude ratio of 1:2 (taken from [HPh1])

the Lissajous figures will encode the phase shift between the two waves in the

later experiment such that one can calculate the wavelength by changing the distances of the mirror. This needs to be done in such a way that the current Lissajous figure (with defined phase difference) transforms into another one with easily determined phase difference. Thus we only consider the red figures (see fig. 6), because for those one can easily determine the phase shift by eye.

2 Experimental procedure

In this section we will present the different setups that were used during the experiment. All setups have been built up using a so called breadboard.

2.1 Measurement of the laser power in dependence of the injection current

First of all it was validated that the height of the laser beam over the optical table is constant. The laser itself and a prism pair have been installed and adjusted by the assistant. The first measurement that was performed during the experiment gives the dependence of the primary laser power on the injection current of the laser. To meausre the power of the fundamental wave the power meter was put into the beam line as seen in fig. 7. The power meter was

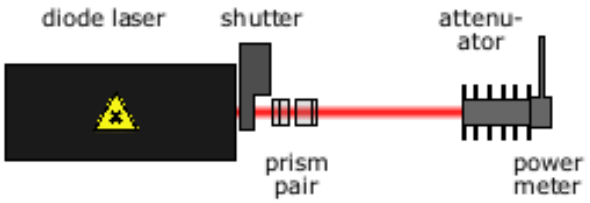

Figure 7: Setup for the characterization of the laser (taken from [A245]

aligned in such a way that it is perpendicular to the beam axis. A straylight-tube is used to shield background radiation. Furthermore it was assured that the beam hits it at the center point of the measuring diode. Since the power meter is only linear up to a power of 20 mW an attenuator has been applied for higher laser powers. The attenuation of this element has been validated with according measurements with and without it. Also here it was crucial to align the attenuator such that it is parallel to the beam. With this setup one can then measure the laser power in dependence of the injection current by altering the latter one in steps of 5 to 10 mA from 0 to 280 mA. The obtained data can be found in tabs. 2 in the appendix and has been plotted[2] in fig. 13. The errors in this table as well as all the other errors, if nothing else is said, result from the number of significant figures of the digital measuring instrument.

[2]All the plots and fits were performed by gnuplot. The errors of the fitting variables used for the further calculations have also been obtained from gnuplot.

2.2 Calibration of the variable attenuator

Since the variation of the laser power using the injection current is not practicable in this experiment a variable attenuator was set up. Therefore a $\lambda/2$-plate and a beam-splitter cube have been installed according to fig. 8 while the injection current was tuned to the maximal value. An accurate alignment of the

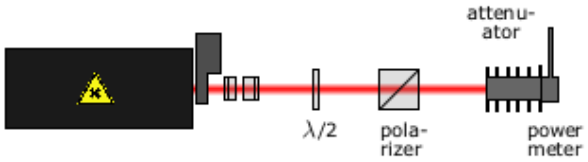

Figure 8: Setup for the calibration of the variable attenuator (taken form [A245])

two elements has to be ensured before measuring. Both elements only affect the polarization of the beam, hence they should not alter the form and direction of the beam. This property can be used to ensure the correct height and angular orientation of the two elements. To follow the infrared laser beam invisible to the eye we used an infrared detection card.
The $\lambda/2$-plate is used as a polarizer and can be rotated around the optical axis, while the beam-splitter also is a polarizer. Hence the theory predicts that the power of the incoming laser beam is attenuated according to Malus law in dependence of the angle between the polarization axes. To validate this behaviour the laser power is measured for angles between 0° and 180° in steps of 2.5°. The obtained data can be found in the appendix in tab. 3.

2.3 Focusing the laser beam into the crystal

For the second harmonic generation the uniaxial crystal potassium niobate ($KNbO_3$) is used that has been heated to a temperature of 36 °C for this adjustment. As described in the theory it is crucial to have an accurately focused beam within the crystal. To achieve this a system of two lenses is installed as seen in fig. 9. At this point the correct alignment of the component is of utterly

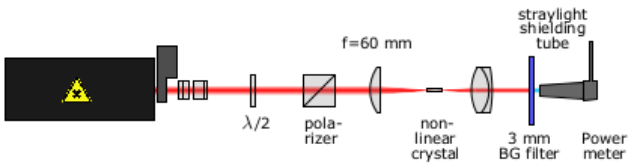

Figure 9: Setup for measuring the intensity of the second harmonic (taken from [A245])

importance, hence it is checked in detail. Since a lens should only change the opening angle of the beam but not the center point this can be used to assure the correct height and angular orientation as described before.
After those two variables have been fixed the distance of the crystal and the two lenses have to be adjusted. The requirement that the beam should be maxim-

ally focused within the crystal and parallel after the second lens yields that each lens should be installed at the distance of their focal length. Hence the coarse adjustment of this length is done using a ruler with millimeter units. The fine adjustment of the lengths can be achieved by observing the beam width after the second length at different (and also far) points along the beam line. It should be constant along the complete path of the beam. During this check a mirror was used to prolong the path of the beam to ensure the correct adjustment of the lengths.

2.4 Optimization of the harmonic power

After the above adjustments the second harmonic could already be observed by the naked eye. Further adjustments have been performed to optimize the output power that was measured with the power meter (installed according to fig. 9). A thick filter was applied to get rid of the fundamental wave allowing us to measure the intensity of the second harmonic beam. First of all the position of the crystal relative to the beam was altered in all three possible directions. The movement in the two directions perpendicular to the beam had the same result. The harmonic power was nearly not influenced by the movement but at had a large drop at the edges of movements in positive and negative direction. This is due to the fact that in this case the edge of the crystal is reached. If one observes the second harmonic by eye this edge is clearly visible within the beam. Thus the displacement in those two directions was chosen to lie in the middle of the interval defined by the appearance of the edge respectively.
In contrast to that nearly binary behaviour the parallel direction showed a smoother one. Moving the crystal along this direction changed the harmonic power much slower. The displacement here was chosen to lie in the point of maximum intensity measured via the power meter.
After the orientation of the crystal within the beam has been fixed, the temperature is altered just a little bit. Here changes of 0.5 °C caused huge changes in the second harmonic power, such that the crystal temperature was left at 36 °C for the time being and was checked later on.
Since the theory states that the second harmonic power massively depends on the fundamental power the orientation of the $\lambda/2$-plate has been changed to maximize the power measured by the power meter. At this time the optimal angle obtained from Malus law was already known and deviations from that previous result did not increase the intensity.
The theory also predicts that the intensity of the second harmonic depends on the polarization of the fundamental wave. However it was not possible to optimize this variable since the orientation of the beam-splitter cube could not be changed.
Finally the temperature of the diode laser was changed, because it is possible that the higher temperature allows access to another mode of the laser and therefore an increase in the power. Unfortunately this had no measurable effect on the second harmonic power at the end of the day.
With these adjustment we achieved a second harmonic power of approximately

25 µW. Later on it turned out that the orientation of the polarization axis of the beam-splitter was indeed not optimal and the power rose to about 50 µW in the polarization measurement. Hence the last two parts of the experiment have been performed without the cube.

2.5 Measurements of the dependencies of the second harmonic power

For the following measurements the setup as described before is used (see fig. 9).

2.5.1 Crystal temperature

For this measurement the crystal is slowly cooled down to 27 °C. It is important to perform the cooling slowly because otherwise tensions could build up within the crystal and tear it apart. When the crystal is cooled down completely the temperature is increased up to 40 °C in steps 0.5 °C. In regions where the harmonic power changed dramatically a smaller step size of 0.2 °C was used. It is important to wait with the measurement until the power changes no longer to account for the time it takes until the crystal is completely heated to the according temperature. This is due to the fact that the coupling of the crystal to the heat bath is not homogeneous but only on the edges, hence it takes some time until the temperature settles down. The according data can be found in tab. 16.
After this measurement the optimal temperature could be deduced, which corresponds to the point of optimal phase matching. Accordingly the crystal temperature was set to this value for the following measurements.

2.5.2 Fundamental wave power

As described before the intensity of the second harmonic depends on the fundamental power. With the built up variable attenuator the power can be altered by rotating the $\lambda/2$-plate. This was done from 0° up to 180° in steps of 2.5°. Data obtained during this measurement can be found in tab. 5.

2.5.3 Polarization of the fundamental wave

To measure the dependence of the second harmonic power on the polarization the beam-splitter cube was removed, otherwise the setup stayed as described in fig. 9. Now the polarization angle of the fundamental wave can be tuned using the $\lambda/2$-plate. The angle was changed from 0° up to 180° in steps of 2.5°. The according data is given in tab. 6 in the appendix.
One important observation of this measurement was that the maximal value of the harmonic power changed from about 25 µW to approximately 50 µW, which can be explained taking into account the polarization axis of the beam-splitter cube. Apparently the polarization of the beam-splitter cube was not optimized relative to the crystal and therefore damped the power of the second harmonic.

2.6 Comparison of the wavelengths with a diffraction grating

Since the intensity is decreasing drastically in the order, we chose to differ from the instructions of the lab course by not putting the beam splitter back in but rather tune the polarization of the fundamental wave to the obtained maximal value. Before installing the grating the second lens was replaced by one with a larger focal length to achieve a broader beam, due to the theoretical dependence of the resolution of the grating on the number of illuminated facets. For the alignment of this lens the same process as described for the other lenses was repeated. After this exchange the grating was installed in such a way that the beam hits it centred. The grating was then rotated such that the zeroth order, easily determined by the intensity, is deflected by an angle of approximately 90°. Now the higher diffraction maxima could be found under larger angles. For each maximum of the two beams the relative distance to the zeroth order maximum was measured.

2.7 Comparison of the wavelengths using a Michelson interferometer

For this measurement the second lens was exchanged back[3]. The complete setup of the interferometer can be seen in fig. 10. After the second lens a thin

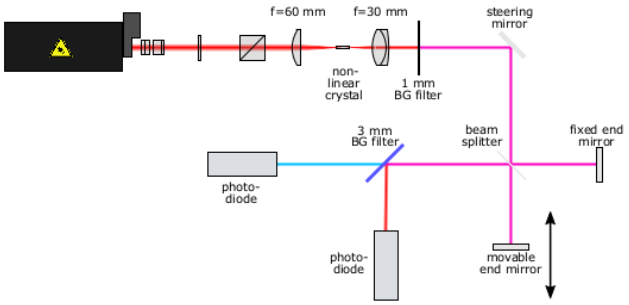

Figure 10: Setup for the measurement with the Michelson interferometer (taken from [A245])

filter is installed to damp the power of the fundamental wave since the used photodiode would be saturated by the full primary power. Further down the optical axis a mirror has been installed. Its azimuthal angle was fixed by rotating it perpendicular to the beam line. In this position the incoming beam should be reflected exactly onto itself. By poking a hole into a piece of paper and holding it such that the primary beam surpasses it before the mirror the two beams can easily be adjusted. Now the mirror is rotated such that it deflects the beam by 90° onto the movable end mirror. Now this mirror can be adjusted using the same trick with the piece of paper as before, but this time both angles have to be fine tuned. When this mirror is completely adjusted the beam-splitter can be

[3]In fact this measurement has been performed before the measurement with the grating in order to minimize potential errors by exchanging the lens.

put into place along with the fixed end mirror. After that the beam-splitter is adjusted such that the deflection angle is 90°. The fixed end mirror is adjusted similar to the other two mirrors. As the last step of the setup the alignment of all beams is checked at a greater distance and the photodiodes are installed. Those have to be adjusted such that the beam hits them centrical. To separate the fundamental wave from the second harmonic the 3mm-filter is used since its transmission of the fundamental wave is nearly zero but the reflection is high enough to use it as a mirror.
Now the two photodiodes can be connected to the oscilloscope which is operated in XY-mode. By slightly bumping against the optical table one can see the change of Lissajous figures on the oscilloscope one of which is exemplary shown in fig. 11. With this setup we can then determine the wavelength relation of the two waves. To do this the mirror is moved such that one of the Lissajous figures discussed in the theory is visible. This displacement is then set to represent zero phase shift. After moving the mirror such that another figure of defined phase shift can be observed the displacement is noted. This process is repeated for as many orders as possible. The obtained data can be found in tab. 7.

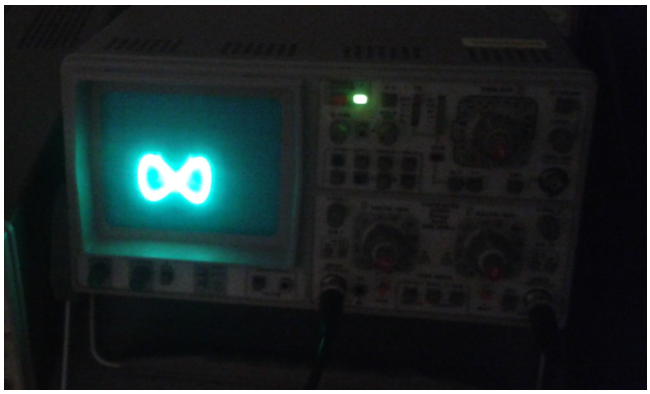

Figure 11: Exemplary Lissajous figure observed by us.

3 Results

3.1 Calibration of the removable attenuator

As we want to compare measurements with and without the removable attenuator the first thing to do is the calibration of this element. It was done by fitting a linear function to the values in tab. 2 measured with and without attenuator. The result is shown in figure 12 and leads to

$$\begin{aligned} P_{\text{att}} &= aP_{\text{dir}} + b \\ &= \frac{0.866 \pm 0.012}{1000} P_{\text{dir}} + 1.01 \pm 0.11 \end{aligned}$$

where P_{att} (P_{dir}) is the intensity of the fundamental beam with (without) attenuator. The fit has a $\chi^2_{\text{red}} = 0.92$ which is an indicator for a good calibration.

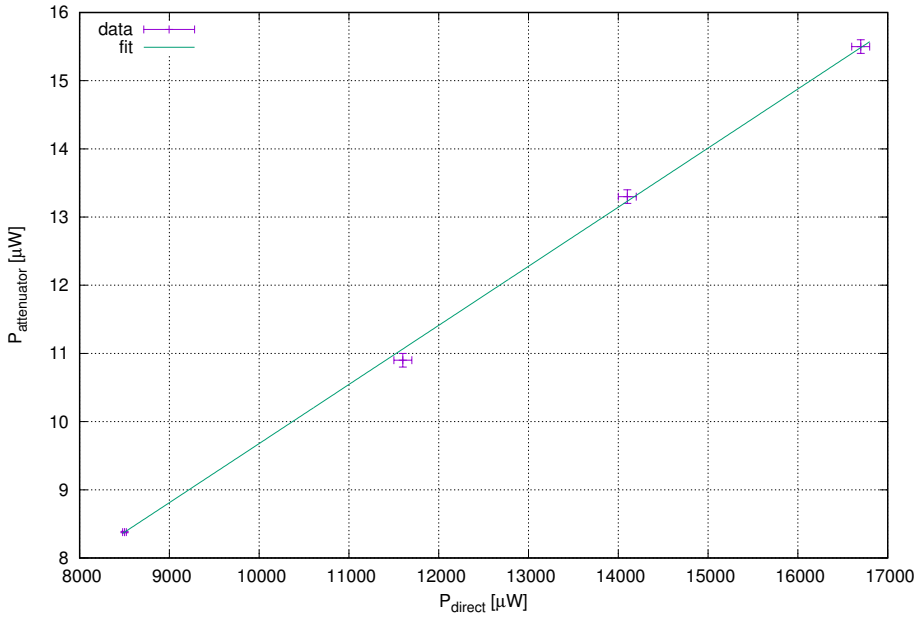

Figure 12: Calibration of the attenuator.

3.2 Dependence of the laser power on the injection current

Now it is possible to calculate the intensity of the beam one would have measured without attenuator

$$\begin{aligned} P_{\text{dir}} &= \frac{P_{\text{att}} - b}{a} \\ \Delta P_{\text{dir}} &= \sqrt{\left(\frac{\Delta P_{\text{att}}}{a}\right)^2 + \left(\frac{\Delta b}{a}\right)^2 + \left(\frac{\Delta a (P_{\text{att}} - b)}{a^2}\right)^2} \end{aligned}$$

where only the statistical error $\Delta P_{\text{att}}/a$ is shown in fig. 13 but the fit[4] of the linearly rising part was performed using the complete error given in tab. 2. It leads to a threshold current $I_{\text{thr}} = (59.32 \pm 0.57)\,\text{A}$ and a linear behaviour above this threshold

$$P_{\text{dir}} = (0.5708 \pm 0.0028)\text{W/A}\; I - (33.86 \pm 0.28)\text{W}\,.$$

With this the differential quantum efficiency can be calculated as

$$\begin{aligned} \eta &= \frac{N_\gamma}{N_e} \\ &= \frac{\partial P}{\partial I}\frac{e\lambda}{hc} \\ &= 0.454 \pm 0.002 \end{aligned}$$

meaning one photon is on average created by $1/\eta = 2.2$ electrons.

[4] Again $\chi^2_{\text{red}} = 1.25$ is very good.

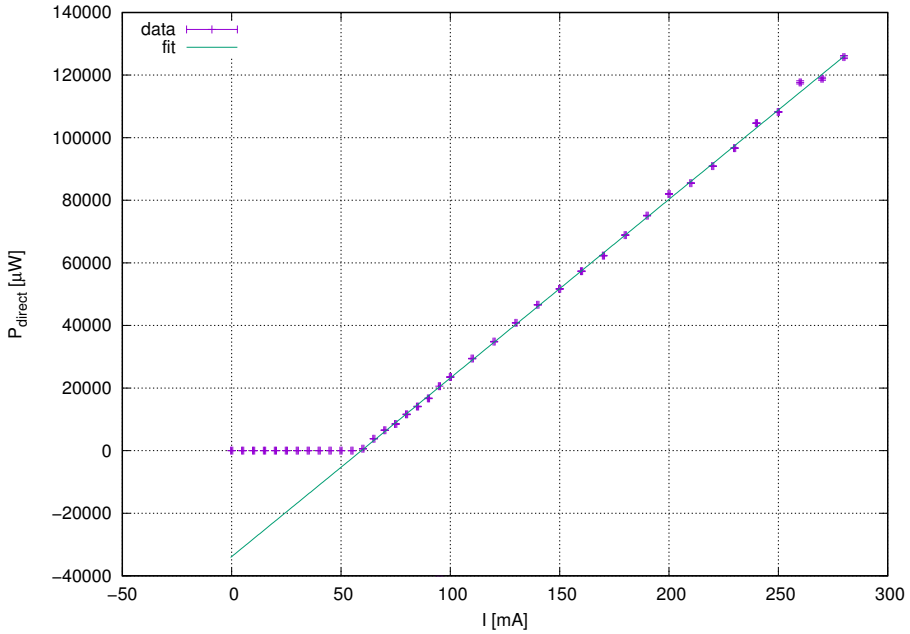

Figure 13: Dependence of the intensity of the fundamental beam on the current.

3.3 Calibration of the variable attenuator

As has already been stated for the following experiments we use a variable attenuator consisting of a $\lambda/2$-plate and a beam-splitter which is expected to follow Malus law. This has been verified by fit to the data in tab. 3 as can be seen in fig. 14. The fitted function is of the form

$$P = P_0 \cos^2\left(\frac{\pi}{180} a(\theta - \theta_0)\right) + P_{\text{off}}$$

where a is expected to be 2 because turning the $\lambda/2$-plate by θ means turning the polarization by 2θ and P_{off} is expected to be a positive and small background. It turns out that we either used too many parameters or overestimated the statistical errors, as $\chi^2_{\text{red}} = 0.28$. The small value is more likely due to second reason because the error for θ was estimated by the fact that the degree-scale had only 5°-marks and we could not be sure on hitting the 2.5°-steps exactly.

The results of the fit are

$$\begin{aligned} P_0 &= (51.74 \pm 0.12)\mu\text{W} \\ a &= 1.9967 \pm 0.0018 \\ \theta_0 &= (25.32 \pm 0.07)^\circ \\ P_{\text{off}} &= (0.28 \pm 0.08)\mu\text{W} \end{aligned}$$

and thus are in very good agreement with the predictions. This leads to an extinction ratio

$$\eta = \frac{P_0 + P_{\text{off}}}{P_{\text{off}}} \pm \sqrt{\left(\frac{\Delta P_0}{P_{\text{off}}}\right)^2 + \left(\frac{P_0 \Delta P_{\text{off}}}{P_{\text{off}}^2}\right)^2} = 186 \pm 53\,.$$

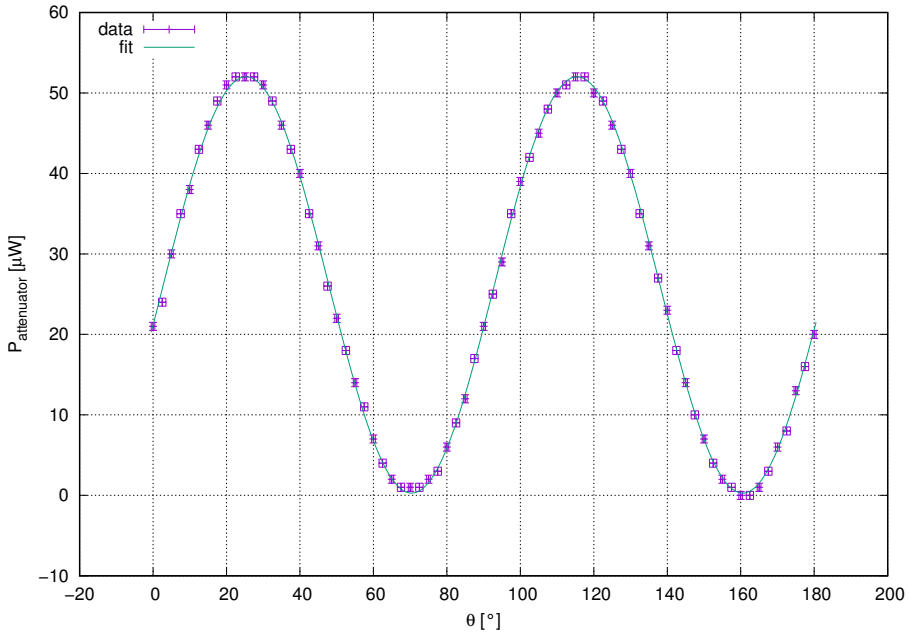

Figure 14: Dependence of the intensity of the fundamental beam on the polarization.

The received function allows to calculate the fundamental intensity very accurately from the angle θ.

3.4 Second harmonic power versus fundamental intensity

Using the calibration obtained in the previous section one can investigate the dependency of the second harmonic power on the fundamental intensity. The needed data is given in tab. 5 where the fundamental intensity reaching the uniaxial crystal is directly given as a result of the previous calculations. The error then is given by

$$\begin{aligned}\Delta P^2 &= \left[2\frac{\pi}{180}aP_0\cos\left(\frac{\pi}{180}a(\theta-\theta_0)\right)\sin\left(\frac{\pi}{180}a(\theta-\theta_0)\right)\Delta\theta\right]^2 \\ &\quad + \left[\cos^2\left(\frac{\pi}{180}a(\theta-\theta_0)\right)\Delta P_0\right]^2 + \Delta P_{\text{off}}^2\end{aligned}$$

where the influence of Δa and $\Delta\theta_0$ can be neglected as they are very small.

Now we can plot the second harmonic power versus fundamental intensity as has been done in fig. 15. Equation 3 suggests a quadratic dependence. Therefore a parabola

$$P_{\text{SH}} = aP_{\text{FUN}}^2 + bP_{\text{FUN}}^2 + c$$

has been fitted to the data. $\chi^2_{\text{red}} = 2.5$ is good enough to consider the hypothesis as validated. In addition the parabola is dominated by the frequency doubling

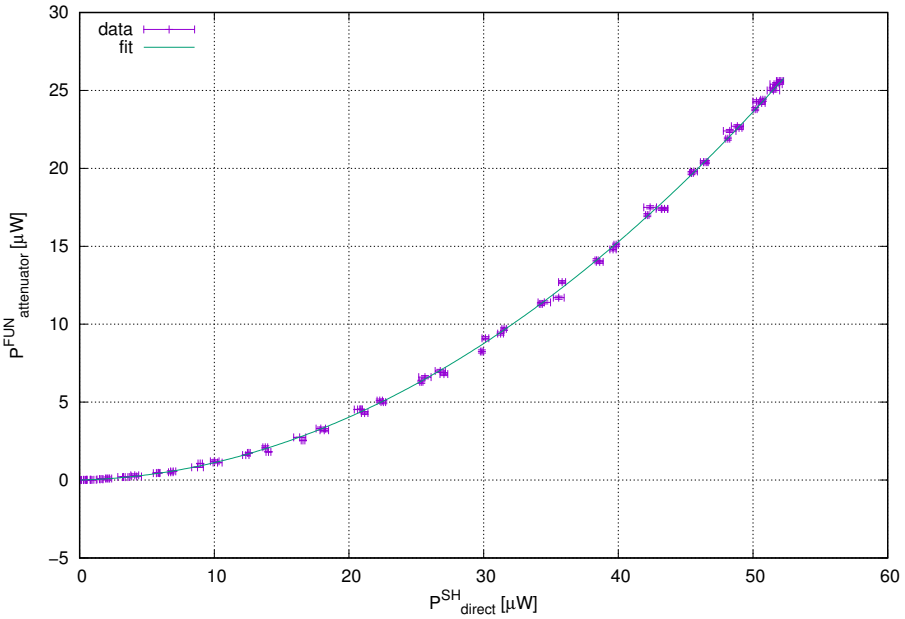

Figure 15: Dependence of the intensity of the second harmonic beam on the fundamental beam power.

efficiency a

$$\begin{aligned} a &= (0.00902 \pm 0.00006)\mu\mathrm{W}^{-1} \\ b &= 0.021 \pm 0.002 \\ c &= (0.002 \pm 0.007)\mu\mathrm{W} \end{aligned}$$

and the parameters b and especially c have huge relative errors. This means that b and c are more or less results of statistical fluctuations and the prediction $I_{\mathrm{SH}} \propto I_{\mathrm{FUN}}$ describes the data.

3.5 Second harmonic power versus crystal temperature

This measurement was performed before the previously described but it was considered sensible to exchange the order in the report. The data containing the intensities of the second harmonic beam depending on the temperature listed in tab. 4 has been visualized in fig. 16. In addition the function introduced in equation 3 has been fitted:

$$P_{\mathrm{SH}} = P_0 \,\mathrm{sinc}^2\left(a\,(T - T_0)\right) + P_{\mathrm{off}}$$

As one can see in fig. 16 and the $\chi^2_{\mathrm{red}} = 6.5$ suggests, only the central peak can

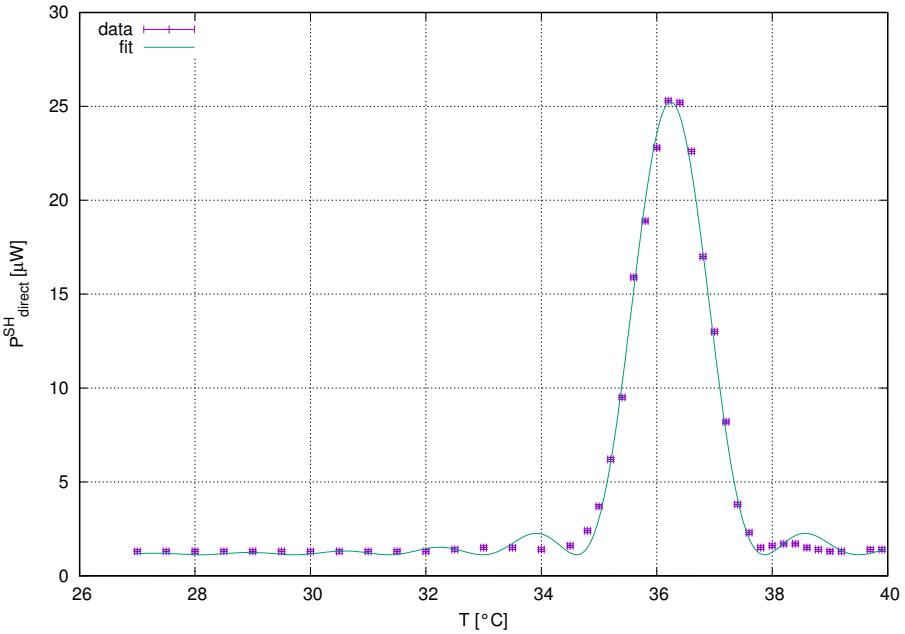

Figure 16: Dependence of the intensity of the second harmonic beam on the temperature.

be described properly by the sinc^2-function with the received parameters

$$\begin{aligned} P_0 &= (24.1 \pm 0.3)\mu\mathrm{W} \\ a &= (1.93 \pm 0.04)\mathrm{K}^{-1} \\ T_0 &= (36.241 \pm 0.030)^\circ\mathrm{C} \\ P_{\mathrm{off}} &= (1.12 \pm 0.06)\mu\mathrm{W}\,. \end{aligned}$$

A possible reason for this behaviour could be a nonlinear dependence of the phase mismatch Δk on the temperature T. This would explain the asymmetry of the data as well as the incoherence between data and fit. But it could not explain the nearly complete absence of secondary maxima. Another reason could be that the crystal did not reach a completely homogeneous temperature. For all the following experiments the temperature $T = 36.3^\circ\mathrm{C}$ has been used. It was chosen as the point between the two highest measured temperatures and is in good accordance with T_0.

3.6 Second harmonic power versus polarization of the fundamental wave

Now that all the calibrations and adjustments have been done and the beamsplitter (which as we remember significantly reduced the second harmonic intensity) has been removed, we can investigate what type of phase matching was achieved. From the theory it is known that we expect

$$P_{\mathrm{SH}} \propto \cos^4\theta \tag{8}$$

as a dependence of the second harmonic intensity on the polarization of the fundamental wave for type I phase matching and

$$P_{\mathrm{SH}} \propto \cos^2\theta \sin^2\theta \tag{9}$$

for type II phase matching. Both dependencies have been fitted to the data in tab. 6 as shown in fig. 17. One can directly see that only the type I matching

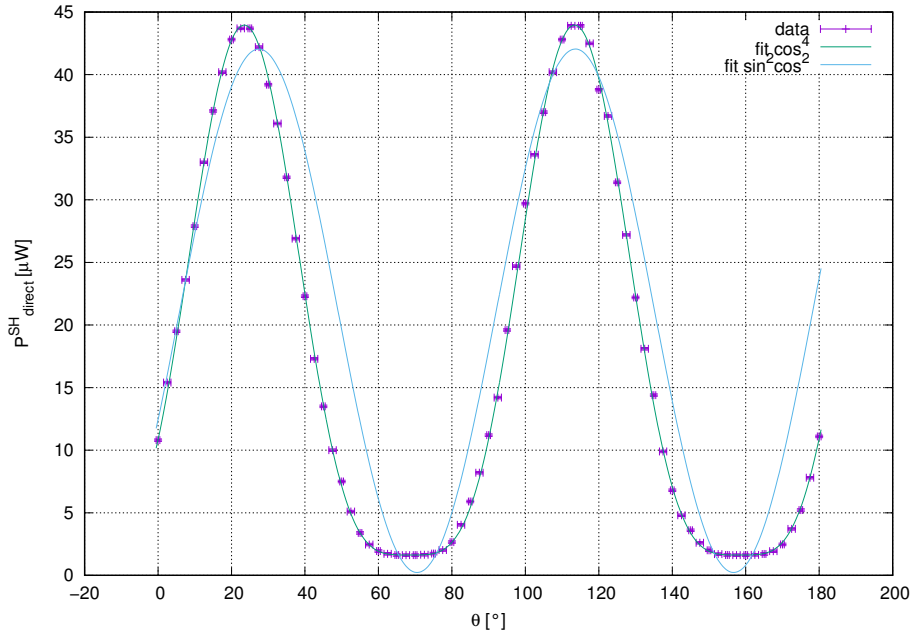

Figure 17: Dependence of the intensity of the second harmonic beam on the polarization of the fundamental beam.

with the $\cos^4$-term describes the data appropriately. The results of this fit[5] are:

$$P_{\mathrm{SH}} = P_0 \cos^4\left(\frac{\pi}{180} a(\theta - \theta_0)\right) + P_{\mathrm{off}} \tag{10}$$

$$P_0 = (42.33 \pm 0.04)\mu\mathrm{W} \tag{11}$$

$$a = 2.0008 \pm 0.0010 \tag{12}$$

$$\theta_0 = (23.45 \pm 0.03)^\circ \tag{13}$$

$$P_{\mathrm{off}} = (1.628 \pm 0.013)\mu\mathrm{W} \tag{14}$$

Again $a = 2$ within errors as expected, thus the result is consistent with the theory for type I phase matching.

3.7 Comparison of the wavelength with a diffraction grating

In fig. 4 a diffraction grating has already been shown. Fig. 18 now shows the arrangement in the experiment performed in order to measure the wavelengths of fundamental and second harmonic beam. The angle $\alpha = \pi/4$ could be achieved in good approximation comparing the angle of incoming and reflected beam with

[5] Again $\chi^2_{\mathrm{red}} = 0.23$ is very small because we overestimated the error of θ.

the holes in the optical table but as any other number it is not exact and we could not find an appropriate error estimation. For any reliable estimation one would have needed better possibilities to measure distances than the measuring stick in our disposition. Therefore we only assumed errors of 0.5 cm on the lengths and rembered the fact that there is at least this additional error source. Simple trigonometry leads to

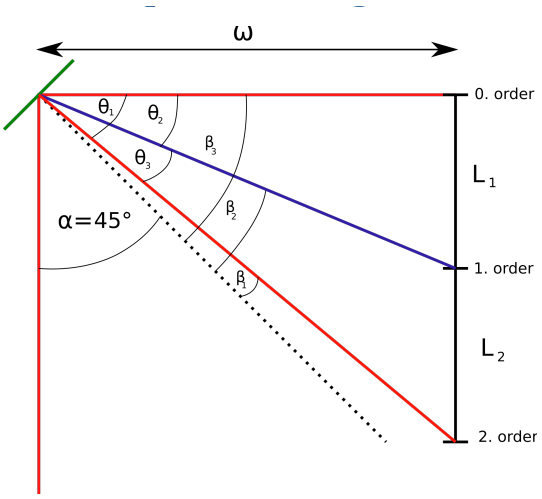

Figure 18: Distances and angles in the arrangement of the grating from [PKZ].

$$\begin{aligned} \theta_m &= \arctan\left(\frac{L_m}{w}\right) \\ \beta_m &= \frac{\pi}{4} - \theta_m \\ s_m &= \sin\alpha - \sin\beta_m \\ \lambda &= \frac{s_m d}{m} \end{aligned}$$

where w is the distance between grating and wall (projection surface), m the order of the maximum, L_m the distance of the m-th maximum to the zeroth, θ_m the corresponding angle, β_m the angle to the normal of the grating, d the facet spacing[6], and s_m an auxiliary variable. The errors then are

$$\begin{aligned} \Delta\theta &= \frac{1}{L^2+w^2}\sqrt{(L\Delta w)^2 + (w\Delta L)^2} \\ \Delta\beta &= \Delta\theta \\ \Delta s &= \cos(\beta)\Delta\beta \\ \Delta\lambda &= \frac{d\Delta s}{m}\,. \end{aligned}$$

The data measured and calculated with $w = 1.335\,\mathrm{m}$ can be found in tab. 1. The literature value for the wavelength of the infrared laser is $\lambda_{\mathrm{FUN}} = 987\,\mathrm{nm}$ and therefore it is expected that the blue second harmonic wave has half its wavelength $\lambda_{\mathrm{SH}} = 493.5\,\mathrm{nm}$. Both 1. order wavelengths calculated in tab. 1 agree with this within the errors and the other two results as well as the error

[6] $d = (600/\mathrm{mm})^{-1}$ taken from [A245].

	L [m]	λ [nm]	$\Delta\lambda$ [nm]	A_{exp}	A_{theo}
1. order SH	0.505	493.2	5.3	92.7	1800
2. order SH	1.05	490.4	2.4	201.3	3600
3. order SH	1.925	491.8	1.2	421.5	5400
1. order FUN	1.055	984.6	4.9	202.4	1800

Table 1: Positions of the maxima of the second harmonic and fundamental beams with corresponding wavelength and experimental as well as theoretical resolution.

weighted mean of the second harmonic wavelength

$$\begin{aligned} \lambda_{\text{SH}} &= \frac{\sum_{m=1}^{3} \frac{\lambda_m}{\Delta\lambda_m^2}}{\sum_{m=1}^{3} \frac{1}{\Delta\lambda_m^2}} \\ \Delta\lambda_{\text{SH}} &= \sqrt{\frac{1}{\sum_{m=1}^{3} \frac{1}{\Delta\lambda_m^2}}} \\ \lambda_{\text{SH}} &= (491.58 \pm 0.96)\text{nm} \end{aligned}$$

lie within a 2σ-interval which is still good enough as this error does not take into account an error on α. An estimation of the ratio between the two wavelengths

$$\begin{aligned} \frac{\lambda_{\text{FUN}}}{\lambda_{\text{SH}}} &= 2.003 \pm 0.011 \\ \Delta\left(\frac{\lambda_{\text{FUN}}}{\lambda_{\text{SH}}}\right) &= \sqrt{\left(\frac{\Delta\lambda_{\text{FUN}}}{\lambda_{\text{SH}}}\right)^2 + \left(\frac{\lambda_{\text{FUN}}\Delta\lambda_{\text{SH}}}{\lambda_{\text{SH}}^2}\right)^2} \end{aligned}$$

reproduces the factor 2 with unexpected accuracy. We seem to have systematically underestimated the wavelength, but do not know how.
In tab. 1 there are two additional columns not mentioned jet. They correspond to the experimental $A_{\text{exp}} = \frac{\lambda}{\Delta\lambda}$ and the theoretical $A_{\text{theo}} = m \cdot N$ resolutions of the grating. The number N of illuminated lines here was estimated by the known spacing 600lines/mm and an approximate width of the laser beam 3 mm, giving $N \approx 1800$. One directly sees that while both resolutions increase nearly proportionally with m, they differ in an order of magnitude. This is easy to understand because in our measurements we were not limited by the optical resolution of the maxima but by our measurement apparatus (i.e. the points were sharp but we could not measure their position properly).

3.8 Comparison of the wavelengths with a Michelson interferometer

Now that we are convinced that the uniaxial crystal is really doing what we want it to do, namely doubling the frequency of the incoming fundamental wave, we can investigate further details. Here the Michelson interferometer is going to give us information on the difference in the refractive index of air depending on the wavelength. The positioning of an adjustable mirror to create different Lissajous figures has already been explained and the results of this measurement can be found in tab. 7 and fig. 19. The plot shows an additional linear fit

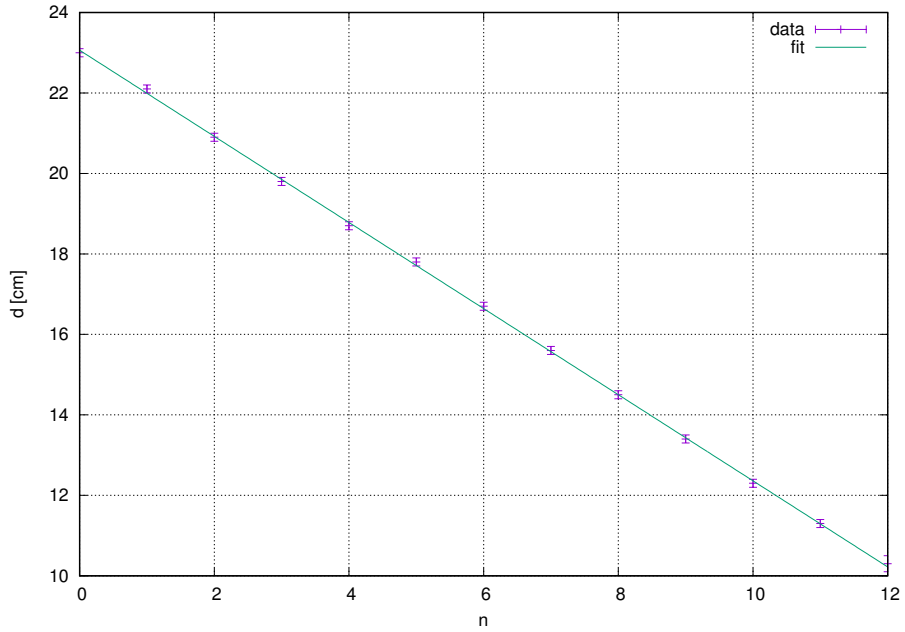

Figure 19: Positions of the adjustable mirror of the Michelson interferometer creating the n-th figure.

function[7]

$$d = an + d_0 \tag{15}$$
$$= (-1.070 \pm 0.005)\text{cm}\, n + (23.06 \pm 0.03)\text{cm} \tag{16}$$

where the sign of the slope as well as the offset of the function are of no interest. They result only from an arbitrarily chosen start of the measurement. The absolute value of the slope gives a clue on the dispersion relation in air. As every step in n is related to a phase difference of $\pi/2$ one gets

$$\frac{\pi}{2} \stackrel{!}{=} \phi_{\text{SH}} - 2\phi_{\text{FUN}} = 2a\,(k_{\text{SH}} - 2k_{\text{FUN}}) = 2a \cdot 2\pi \left(\frac{2n_{\text{SH}}}{2\lambda_{\text{SH}}} - \frac{2n_{\text{FUN}}}{\lambda_{\text{FUN}}} \right) \approx 8\pi a \frac{n_{\text{SH}} - n_{\text{FUN}}}{\lambda_{\text{FUN}}}$$

and therefore

$$n_{\text{SH}} - n_{\text{FUN}} = \frac{\lambda_{\text{FUN}}}{16a}$$
$$\Delta\,(n_{\text{SH}} - n_{\text{FUN}}) = \frac{\lambda_{\text{FUN}} \Delta a}{16a^2}\,.$$

In the calculation above the phase ϕ and the wave vector k were used and λ always denotes the wavelength in vacuum. Plugging in the numbers leads to

$$n_{\text{SH}} - n_{\text{FUN}} = (5.765 \pm 0.027) \cdot 10^{-6}\,.$$

[7] $\chi^2_{\text{red}} = 0.40$ is good enough.

In [A245] the formula

$$\begin{aligned} s &= \frac{1}{\lambda[\mu\mathrm{m}]} \\ 10^8(n-1) &= 8342.13 + \frac{2406030}{130 - s^2} + \frac{15997}{38.9 - s^2} \end{aligned} \tag{17}$$

is given in order to calculate the theoretical difference in the refractive indices. It gives $n_{\mathrm{SH}} - n_{\mathrm{FUN}} = 4.937 \cdot 10^{-6}$ which is far beyond any error intervals from our value. We can not definitely say what caused this discrepancy but the day on which we performed the experiment was very warm and we did not measure air pressure nor humidity. It is probable that these variables had an influence on the refractive indices.
The difference between the refractive indices is in the same time the deviation from the exact 2:1 ratio of fundamental and second harmonic wave. The calculation of the difference in wavelength is nearly as trivial because all refractive indices are approximately one:

$$\begin{aligned} \lambda_{\mathrm{FUN}} - 2\lambda_{\mathrm{SH}} &= \lambda_{\mathrm{FUN}} \left(\frac{1}{n_{\mathrm{FUN}}} - \frac{1}{n_{\mathrm{SH}}} \right) \approx \lambda_{\mathrm{FUN}} \left(n_{\mathrm{SH}} - n_{\mathrm{FUN}} \right) \\ \Delta \left(\lambda_{\mathrm{FUN}} - 2\lambda_{\mathrm{SH}} \right) &= \lambda_{\mathrm{FUN}} \Delta \left(n_{\mathrm{SH}} - n_{\mathrm{FUN}} \right) \\ \lambda_{\mathrm{FUN}} - 2\lambda_{\mathrm{SH}} &= (5.69 \pm 0.03)\mathrm{pm} \end{aligned}$$

This allows us to deduce the spectroscopical resolution $A = \frac{\lambda_{\mathrm{SH}}}{\Delta\lambda} = 86727 \pm 405$ of the interferometer[8]. As one would have expected it is much greater than the resolution of the grating.

4 Conclusion

This experiment gave a us a deep insight into non-linear aspects as well as general issues of optics. It was our first advanced optics experiment and thus helped us a lot in understanding adjustment and calibration of optical elements.
A diode laser has been inspected and it showed the characteristic dependence on the injection current, namely nearly no power until a threshold and then linear dependence. In addition a calibration of two different attenuators has been carried out successfully.
The main goal of the experiment was achieved by building up a system creating blue light out of infrared using frequency doubling. The efficiency was satisfying in spite of the fact that the beam-splitter could not be rotated and led to a loss of nearly half the intensity. We could confirm that the second harmonic beam intensity depends quadratically on the fundamental power and has a sinc^2-dependence on the phase mismatch changed via temperature. The sinc^2-dependence was very good around the main maximum but not exact away from it.
As the dependence of the second harmonic intensity on the polarization of the fundamental wave follows exactly a $\cos^4$-distribution, we could identify type I

[8] $\Delta A = \frac{\lambda_{\mathrm{SH}} \Delta\Delta\lambda}{\Delta\lambda^2}$

phase matching.
Two different methods were used to investigate the 2:1 wavelength ratio. The measurement with a diffraction grating lead to a confirmation of the ratio but it did not have a high resolution. In contrast very accurate measurements could be performed using a Michelson interferometer. They again implied a 2:1 ratio of the frequencies but in addition allowed an investigation of the refractive index of air depending on the wavelength. The result of this investigation does not agree with the theory and we can only assume that temperature or other influences changed the refractive index of air significantly.
All in all the experiment was successful and even the two parts that did not exactly agree with the theory, namely the sinc^2-dependence of the second harmonic power on the temperature and wavelength dependence of the refractive index of air, still gave results within the expected order of magnitude.

A Data: Laser power versus injection current

I [mA]	ΔI [mA]	P_{direct} [µW]	ΔP_{direct} [µW]	$P_{\text{attenuator}}$ [µW]	$\Delta P_{\text{attenuator}}$ [µW]
0	0.5	0.1	0.01		
5	0.5	0.68	0.01		
10	0.5	1.85	0.01		
15	0.5	3.2	0.01		
20	0.5	4.68	0.01		
25	0.5	6.16	0.01		
30	0.5	7.97	0.01		
35	0.5	10	0.1		
40	0.5	12.4	0.1		
45	0.5	15.2	0.1		
50	0.5	18.6	0.1		
55	0.5	22.8	0.1		
60	0.5	600	20		
65	0.5	3790	20		
70	0.5	6520	20		
75	0.5	8500	20	8.38	0.01
80	0.5	11600	100	10.9	0.1
85	0.5	14100	100	13.3	0.1
90	0.5	16700	100	15.5	0.1
95	0.5	20600	100		
100	0.5	23525	383	21.4	0.1
110	0.5	29409	461	26.5	0.1
120	0.5	34832	535	31.2	0.1
130	0.5	40832	618	36.4	0.1
140	0.5	46601	699	41.4	0.1
150	0.5	51678	771	45.8	0.1
160	0.5	57332	851	50.7	0.1
170	0.5	62293	922	55	0.1
180	0.5	68870	1016	60.7	0.1
190	0.5	75100	1105	66.1	0.1
200	0.5	82023	1205	72.1	0.1
210	0.5	85485	1255	75.1	0.1
220	0.5	90908	1333	79.8	0.1
230	0.5	96677	1416	84.8	0.1
240	0.5	104638	1531	91.7	0.1
250	0.5	108215	1583	94.8	0.1
260	0.5	117676	1810	103	0.5
270	0.5	118830	1826	104	0.5
280	0.5	125753	1921	110	0.5

Table 2: Intensity of the fundamental beam at different currents with and without attenuator. The "direct"-data below the free line is not measured but calculated according to the calibration.

B Data: Calibration of the variable attenuator

θ [°]	$\Delta\theta$ [°]	P [µW]	ΔP [µW]	θ [°]	$\Delta\theta$ [°]	P [µW]	ΔP [µW]
0	0.5	21	0.5	92.5	1	25	0.5
2.5	1	24	0.5	95	0.5	29	0.5
5	0.5	30	0.5	97.5	1	35	0.5
7.5	1	35	0.5	100	0.5	39	0.5
10	0.5	38	0.5	102.5	1	42	0.5
12.5	1	43	0.5	105	0.5	45	0.5
15	0.5	46	0.5	107.5	1	48	0.5
17.5	1	49	0.5	110	0.5	50	0.5
20	0.5	51	0.5	112.5	1	51	0.5
22.5	1	52	0.5	115	0.5	52	0.5
25	0.5	52	0.5	117.5	1	52	0.5
27.5	1	52	0.5	120	0.5	50	0.5
30	0.5	51	0.5	122.5	1	49	0.5
32.5	1	49	0.5	125	0.5	46	0.5
35	0.5	46	0.5	127.5	1	43	0.5
37.5	1	43	0.5	130	0.5	40	0.5
40	0.5	40	0.5	132.5	1	35	0.5
42.5	1	35	0.5	135	0.5	31	0.5
45	0.5	31	0.5	137.5	1	27	0.5
47.5	1	26	0.5	140	0.5	23	0.5
50	0.5	22	0.5	142.5	1	18	0.5
52.5	1	18	0.5	145	0.5	14	0.5
55	0.5	14	0.5	147.5	1	10	0.5
57.5	1	11	0.5	150	0.5	7	0.5
60	0.5	7	0.5	152.5	1	4	0.5
62.5	1	4	0.5	155	0.5	2	0.5
65	0.5	2	0.5	157.5	1	1	0.5
67.5	1	1	0.5	160	0.5	0	0.5
70	0.5	1	0.5	162.5	1	0	0.5
72.5	1	1	0.5	165	0.5	1	0.5
75	0.5	2	0.5	167.5	1	3	0.5
77.5	1	3	0.5	170	0.5	6	0.5
80	0.5	6	0.5	172.5	1	8	0.5
82.5	1	9	0.5	175	0.5	13	0.5
85	0.5	12	0.5	177.5	1	16	0.5
87.5	1	17	0.5	180	0.5	20	0.5
90	0.5	21	0.5				

Table 3: Intensity of the fundamental beam at different polarizations measured with attenuator.

C Data: Harmonic intensity versus crystal temperature

T [°C]	ΔT [°C]	P [µW]	ΔP [µW]
27	0.05	1.3	0.1
27.5	0.05	1.3	0.1
28	0.05	1.3	0.1
28.5	0.05	1.3	0.1
29	0.05	1.3	0.1
29.5	0.05	1.3	0.1
30	0.05	1.3	0.1
30.5	0.05	1.3	0.1
31	0.05	1.3	0.1
31.5	0.05	1.3	0.1
32	0.05	1.3	0.1
32.5	0.05	1.4	0.1
33	0.05	1.5	0.1
33.5	0.05	1.5	0.1
34	0.05	1.4	0.1
34.5	0.05	1.6	0.1
34.8	0.05	2.4	0.1
35	0.05	3.7	0.1
35.2	0.05	6.2	0.1
35.4	0.05	9.5	0.1
35.6	0.05	15.9	0.1
35.8	0.05	18.9	0.1
36	0.05	22.8	0.1
36.2	0.05	25.3	0.1
36.4	0.05	25.2	0.1
36.6	0.05	22.6	0.1
36.8	0.05	17	0.1
37	0.05	13	0.1
37.2	0.05	8.2	0.1
37.4	0.05	3.8	0.1
37.6	0.05	2.3	0.1
37.8	0.05	1.5	0.1
38	0.05	1.6	0.1
38.2	0.05	1.7	0.1
38.4	0.05	1.7	0.1
38.6	0.05	1.5	0.1
38.8	0.05	1.4	0.1
39	0.05	1.3	0.1
39.2	0.05	1.3	0.1
39.7	0.05	1.4	0.1
39.9	0.05	1.4	0.1

Table 4: Intensity of the second harmonic beam at different temperatures measured without attenuator.

D Data: Harmonic power versus fundamental power

θ [°]	$\Delta\theta$ [°]	P_{SH}	ΔP_{SH}	P_{FUN}	ΔP_{FUN}	θ [°]	$\Delta\theta$ [°]	P_{SH}	ΔP_{SH}	P_{FUN}	ΔP_{FUN}
0	0.5	4.3	0.1	21.17	0.24	92.5	1	6.3	0.1	25.37	0.12
2.5	1	6.6	0.1	25.64	0.46	95	0.5	8.25	0.1	29.87	0.11
5	0.5	9.1	0.1	30.13	0.25	97.5	1	11.3	0.1	34.25	0.12
7.5	1	11.4	0.1	34.50	0.47	100	0.5	14.1	0.1	38.39	0.12
10	0.5	14	0.1	38.62	0.26	102.5	1	17	0.1	42.15	0.13
12.5	1	17.5	0.1	42.36	0.47	105	0.5	19.7	0.1	45.43	0.13
15	0.5	19.8	0.1	45.61	0.26	107.5	1	21.9	0.1	48.13	0.15
17.5	1	22.4	0.1	48.27	0.47	110	0.5	23.8	0.1	50.16	0.15
20	0.5	24.3	0.1	50.26	0.26	112.5	1	25.1	0.1	51.47	0.17
22.5	1	25	0.1	51.52	0.47	115	0.5	25.6	0.1	52.00	0.16
25	0.5	25.6	0.1	52.01	0.26	117.5	1	25.4	0.1	51.76	0.19
27.5	1	25.4	0.1	51.72	0.46	120	0.5	24.4	0.1	50.73	0.16
30	0.5	24.2	0.1	50.65	0.26	122.5	1	22.6	0.1	48.97	0.22
32.5	1	22.7	0.1	48.84	0.44	125	0.5	20.4	0.1	46.51	0.16
35	0.5	20.4	0.1	46.34	0.25	127.5	1	17.4	0.1	43.44	0.24
37.5	1	17.4	0.1	43.24	0.42	130	0.5	15.1	0.1	39.84	0.16
40	0.5	14.8	0.1	39.61	0.23	132.5	1	12.7	0.1	35.83	0.26
42.5	1	11.7	0.1	35.58	0.40	135	0.5	9.7	0.1	31.52	0.17
45	0.5	9.4	0.1	31.26	0.22	137.5	1	6.8	0.1	27.05	0.29
47.5	1	7	0.1	26.78	0.38	140	0.5	5	0.1	22.56	0.17
50	0.5	5.1	0.1	22.29	0.20	142.5	1	3.2	0.1	18.17	0.31
52.5	1	3.3	0.1	17.91	0.35	145	0.5	1.81	0.01	14.02	0.18
55	0.5	2.1	0.1	13.79	0.18	147.5	1	1.12	0.01	10.24	0.34
57.5	1	1.2	0.1	10.03	0.32	150	0.5	0.56	0.01	6.95	0.19
60	0.5	0.5	0.1	6.77	0.17	152.5	1	0.23	0.01	4.23	0.36
62.5	1	0.3	0.1	4.09	0.29	155	0.5	0.1	0.01	2.18	0.20
65	0.5	0.1	0.1	2.08	0.15	157.5	1	0.02	0.01	0.85	0.39
67.5	1	0.02	0.01	0.80	0.26	160	0.5	0.003	0.01	0.29	0.21
70	0.5	0.008	0.01	0.29	0.14	162.5	1	0.01	0.01	0.52	0.41
72.5	1	0.016	0.01	0.55	0.23	165	0.5	0.042	0.01	1.52	0.22
75	0.5	0.068	0.01	1.60	0.13	167.5	1	0.2	0.01	3.26	0.42
77.5	1	0.19	0.01	3.39	0.20	170	0.5	0.44	0.01	5.70	0.23
80	0.5	0.46	0.01	5.86	0.11	172.5	1	0.82	0.01	8.76	0.44
82.5	1	1.06	0.01	8.96	0.16	175	0.5	1.6	0.01	12.34	0.23
85	0.5	1.74	0.01	12.57	0.10	177.5	1	2.74	0.01	16.34	0.45
87.5	1	2.54	0.01	16.59	0.14	180	0.5	4.53	0.01	20.64	0.24
90	0.5	4.54	0.01	20.90	0.10						

Table 5: Intensity of the second harmonic beam at different polarizations measured without attenuator and corresponding intensities of the fundamental beam (with attenuator). All intensities in µW.

E Data: Harmonic intensity versus fundamental polarization

θ [°]	$\Delta\theta$ [°]	P [µW]	ΔP [µW]	θ [°]	$\Delta\theta$ [°]	P [µW]	ΔP [µW]
0	0.5	10.8	0.1	92.5	1	14.2	0.1
2.5	1	15.4	0.1	95	0.5	19.6	0.1
5	0.5	19.5	0.1	97.5	1	24.7	0.1
7.5	1	23.6	0.1	100	0.5	29.7	0.1
10	0.5	27.9	0.1	102.5	1	33.6	0.1
12.5	1	33.0	0.1	105	0.5	37	0.1
15	0.5	37.1	0.1	107.5	1	40.2	0.1
17.5	1	40.2	0.1	110	0.5	42.8	0.1
20	0.5	42.8	0.1	112.5	1	43.9	0.1
22.5	1	43.7	0.1	115	0.5	43.9	0.1
25	0.5	43.7	0.1	117.5	1	42.5	0.1
27.5	1	42.2	0.1	120	0.5	38.8	0.1
30	0.5	39.2	0.1	122.5	1	36.7	0.1
32.5	1	36.1	0.1	125	0.5	31.4	0.1
35	0.5	31.8	0.1	127.5	1	27.2	0.1
37.5	1	26.9	0.1	130	0.5	22.2	0.1
40	0.5	22.3	0.1	132.5	1	18.1	0.1
42.5	1	17.3	0.1	135	0.5	14.4	0.1
45	0.5	13.5	0.1	137.5	1	9.9	0.1
47.5	1	10.0	0.1	140	0.5	6.8	0.1
50	0.5	7.5	0.1	142.5	1	4.8	0.1
52.5	1	5.1	0.1	145	0.5	3.6	0.1
55	0.5	3.39	0.1	147.5	1	2.6	0.1
57.5	1	2.46	0.1	150	0.5	2	0.1
60	0.5	1.94	0.1	152.5	1	1.7	0.1
62.5	1	1.72	0.1	155	0.5	1.63	0.1
65	0.5	1.63	0.1	157.5	1	1.62	0.1
67.5	1	1.62	0.1	160	0.5	1.62	0.1
70	0.5	1.62	0.1	162.5	1	1.64	0.1
72.5	1	1.65	0.1	165	0.5	1.71	0.1
75	0.5	1.74	0.1	167.5	1	1.93	0.1
77.5	1	2.02	0.1	170	0.5	2.47	0.1
80	0.5	2.66	0.1	172.5	1	3.71	0.1
82.5	1	4.04	0.1	175	0.5	5.22	0.1
85	0.5	5.9	0.1	177.5	1	7.8	0.1
87.5	1	8.2	0.1	180	0.5	11.1	0.1
90	0.5	11.2	0.1				

Table 6: Intensity of the second harmonic beam at different polarizations of the fundamental beam measured without attenuator.

F Data: Michelson interferometer

n	d [cm]	Δd [cm]	figure
0	23.0	0.1	eight
1	22.1	0.1	down parabola
2	20.9	0.1	eight
3	19.8	0.1	up parabola
4	18.7	0.1	eight
5	17.8	0.1	down parabola
6	16.7	0.1	eight
7	15.6	0.1	up parabola
8	14.5	0.1	eight
9	13.4	0.1	down parabola
10	12.3	0.1	eight
11	11.3	0.1	up parabola
12	10.3	0.2	eight

Table 7: Positions of the adjustable mirror of the Michelson interferometer creating the corresponding figure.

List of Figures

List of Tables

References

[A245] Advanced Physics Laboratory Course Part II: Experiment Description for A245 Optical Frequency doubling

[LSP] Stefan Linden: Lecture Notes on Photonic Devices, 2016

[MOLL] Dieter Meschede: Optik, Licht und Laser, Chapter 12, Wiley VCH, Weinheim, 2007

[WGB] `https://en.wikipedia.org/wiki/Gaussian_beam#/media/File:GaussianBeamWaist.svg` - Last accessed on 25th of June

[WikiG] `https://en.wikipedia.org/wiki/Blazed_grating#/media/File:Blazed_grating.svg` - Last accessed on 25th of June

[PKZ] Michael Kajan, Yan Zhiqiang: Physics 601 Advanced Lab Course Report, Optical Frequency Doubling

[WAT] `https://en.wikipedia.org/wiki/Aether_theories` - Last accessed on 25th of June

[WiMM] `https://en.wikipedia.org/wiki/Michelson_interferometer#/media/File:Michelson_interferometer_with_labels.svg` - Last accessed on 25th of June

[HPh1] `web.physik.rwth-aachen.de/~hebbeker/lectures/ph1_0102/p112_l05.htm` - Last accessed during the first year of Bachelor studies - annoyingly the website is down by now